Evaluation of Contra-Rotating Flux-Modulated Machine Featured with Dual Flux-Modulation for Wind Power Generation

Hao Chen, *Member, IEEE*, Ayman M. EL-Refaie, *Fellow, IEEE*, Yuefei Zuo, *Member, IEEE*, Shun Cai, *Member, IEEE*, Shuangchun Xie, and Christopher H. T. Lee, *Senior Member, IEEE*

***Abstract*—This paper presents an investigation and evaluation of an integrated flux-modulated machine for wind power generation. The integrated flux-modulated machine has two rotors which functions two contra-rotating rotors connected with two turbine blades. Hence, compared to conventional wind generators, more wind energy can be captured by this wind power generation system. Moreover, the integrated machine consists of two sets of stator windings. By regulating the currents in these windings, dual maximum power point tracking (MPPT) control strategy can be achieved. As a result, the wind power conversion efficiency is further improved. Moreover, this wind power generation system exhibits the advantage of high torque/power density due to the enhanced magnetic-gearing effect involved in the integrated flux-modulated machine. Hence, this machine is more suitable for direct-drive wind power generation, where the reliability is improved without the maintenance issues caused by mechanical gearboxes. The topology and operating principle of the investigated machine are demonstrated in detail. Decoupled design of the two sets of windings is investigated, and a general rule to achieve decoupled windings by appropriate slot-pole combination selection is illustrated. The advantages of the investigated machine are confirmed in comparison with a benchmark machine. Finally, the investigated flux-modulated machine is prototyped. The validity of the operating principle and the simulation results are verified by experimental results.**

***Index Terms*—Contra-rotating, flux-modulation, magnetic-geared machine, wind power generation.**

I. Introduction

With the ever-increasing concerns on environmental protection and energy crisis, focus on worldwide energy generation has been shifting from fossil fuels to renewable energy sources, such as wind, solar, biofuels, and tidal streams. Among them, wind power generation is the completely clean and sustainable, as well as the fast-growing renewable energy source that has been gaining interest in both industry and academia [1], [2].

Electric machines are the key enabling technology for wind power generation. The required basic performance metrics of an electric machine for wind power generation systems include high torque/power density, high efficiency, high reliability, low cost, as well as flexible controllability [3]. To target the mentioned objectives, various types of electric machines have been developed as wind generators. Compared to conventional squirrel-cage induction machines and wound-rotor induction machines, doubly-fed induction machines have attracted more interest as commercially-available products in modern wind turbine market, *e.g.*, Vestas V80 (2.0 MW) and Siemens/Gamesa 145 (5.0 MW), due to the advantages of improved reliability, flexible control of active and reactive power, and improved low voltage ride-through. However, such machines suffer from low torque density, low efficiency, and relatively complicated power control [4]. With the development of permanent magnet materials and power electronic devices, permanent magnet synchronous machines (PMSMs) have become the most promising candidate in wind power generation applications due to their inherently high torque density, high efficiency, and high reliability [5], [6]. Since the output torque of conventional PMSMs is limited by the machine size, such generators, *e.g.*, Vestas V90 (2.0 MW), are typically working in high-speed operation in order to improve the power density. Hence, a reduction gearbox is typically required to match the low-speed wind to the high-speed generator, which leads to heaviness and bulkiness, noise and vibration, regular maintenance requirement, reduced efficiency, and high cost.

With the aim to eliminate the gearbox by improving torque density associated techniques, a number of new entrants/ variants of PMSMs based on flux modulation theory are emerging for gearless direct-drive wind power generation applications, including flux-switching PM machines [7], [8], flux-reversal PM machines [9], Vernier PM machines [10], and magnetic-geared PM machines [11], [12], [13]. Among them, the magnetic-geared PM machines outperform other counterparts in terms of the torque density, PM utilization ratio, cost, and produced power quality, which makes them more suitable for direct-drive wind generators [14]. A magnetic-geared machine for direct-drive wind power generation is presented in [15], which artfully incorporates a magnetic gear into an inner-rotor PMSM. Hence, there is a steady torque boost as a reduction mechanical gear does, leading to achieve low-speed high-torque direct-drive function, which is favorable for wind power generation applications. It is found that the presented magnetic-geared machine outperforms the PMSM counterpart across the entire range of torque density and efficiency. A double-stator magnetic-geared PM machine for

wind power generation is presented in [16]. It is shown that by utilizing the modulation-ring structure, this machine can modulate the high-speed rotating armature field of the two stators to match the low-speed rotating PM field of the rotor. Hence, this machine readily achieves the low-speed high-torque merit. However, the multi-slot structure brings challenges in winding coils and manufacturing process. Another double-stator magnetic-geared machine is presented in [17], whose inner stator is wound by field windings while the armature windings are located in the outer stator. The pole-pair number of the inner excitation sources can be flexibly changed through injecting variable DC filed currents, which is desirable to match the varying wind speed. Moreover, an effective magnetic field adjustment can be achieved by regulating the dominant pole-pair flux components. Hence, the torque density and flux-regulation capability of this machine are both improved.

Building upon the existing magnetic-geared machines, this paper brings new contributions by presenting an integrated flux-modulated machine for direct-drive wind power generation. The integrated flux-modulated machine has two rotors which functions two contra-rotating rotors connected with two turbine blades. Hence, more wind energy can be captured by this wind power generation system. Moreover, the integrated machine consists of two sets of stator windings. By regulating the currents in these windings, dual maximum power point tracking (MPPT) control strategy can be achieved. As a result, the wind power convention efficiency is further improved. Moreover, the integrated flux-modulated machine exhibits the advantage of high torque density due to the enhanced magnetic-gearing effect.

II. System Configuration and Operating Principle

A. Contra-Rotating Wind Power System

The contra-rotating wind turbine concept was firstly patented in [18]. It was subsequently developed for a 30 kW contra-rotating wind turbine in [19], as shown in Fig. 1. The combined torque from the two contra-rotating rotors is transmitted to the sun gear through the bevel-planetary gearbox. Then it drives the generator in the vertical axis to generate electricity. It was shown that with such two contra-rotating blades, up to 40% more wind energy could be captured and converted into electric energy, compared to conventional wind turbines with a single blade [20]. However, the mechanical gearbox inevitably suffers from the demerits of regular maintenance requirement, bulkiness, acoustic noise, low reliability, and high cost, etc. Moreover, the torque split ratio on the two rotor shafts remains constant due to the fixed gear ratio of such gearbox. As a result, the MPPT control strategy on both rotor shafts is impossible.

In order to solve the mentioned issues, a gearless direct-drive contra-rotating wind power generation system based on an integrated flux-modulated machine is proposed, as shown in Fig. 2. The integrated flux-modulated machine will be illustrated in detail in the following sections. As can be seen, the outer rotor rotating in counter-clockwise direction is directly connected to the main turbine, while the inner rotor rotating in clockwise direction is directly connected to the auxiliary turbine in order to capture more wind energy. Moreover, due to the fact that the two rotors are rotating in opposite directions, the relative angular speed of the two rotors and the relative angular velocity of the rotating magnetic field in the air-gap are increased. Hence, the frequency of the induced voltage/current is increased based on the Faraday's Law, which is desirable for low-speed direct-drive wind power generators. In addition, the torques on the two rotors can be flexibly controlled by the two sets of windings, *i.e.*, Winding I and Winding II, respectively. Hence, dual MPPT control strategy can be achieved, which maximizes the wind energy conversion efficiency.

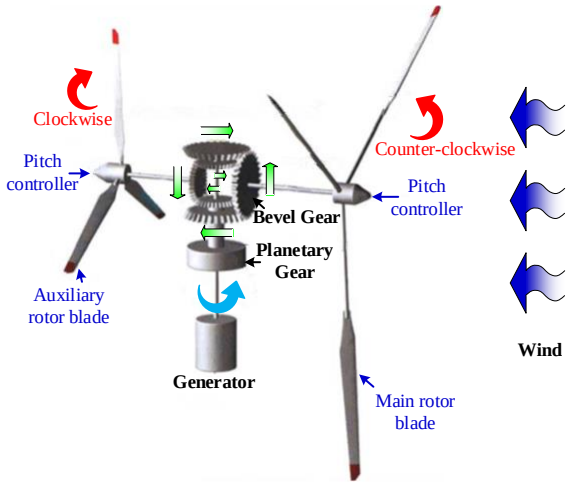

Fig. 1. Conventional contra-rotating wind generator system installed with bevel-planetary gear [19].

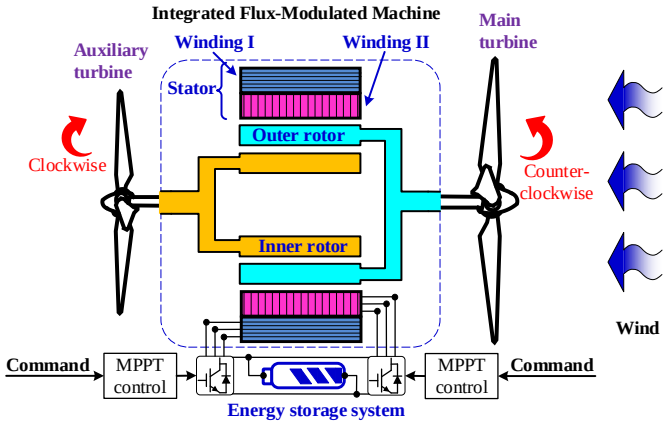

Fig. 2. Gearless direct-drive contra-rotating wind generator system.

B. The Integrated Flux-Modulated Machine Topology

The topology of the integrated flux-modulated machine is shown in Fig. 3. As can be seen, there are two sets of windings in the stator, *i.e.*, winding I and winding II. More specifically, the outer stator teeth are wound by winding I, while the inner stator teeth are wound by winding II. The outer rotor consists of PMs and steel segments. These PMs are circumferentially

magnetized with alternatively opposite polarity, between which steel segments are sandwiched. The inner rotor is a salient rotor

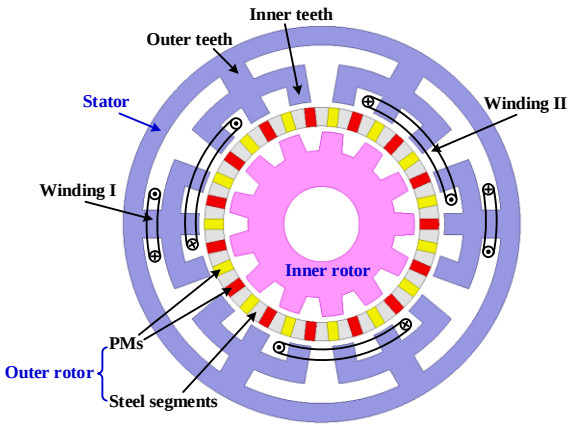

Fig. 3. Topology of the integrated flux-modulated machine.

with the features of simple structure and mechanical robustness, which is identical to those of conventional switched reluctance motors. The main parameters of the integrated flux-modulated machine are listed in Table I.

C. Operating Principle

The integrated flux-modulated machine consists of two parts, *i.e.*, magnetic-geared PM machine part and Vernier PM machine part. More specifically, winding I on the outer stator teeth, PMs in the outer rotor, and the inner rotor constitute a magnetic-geared machine, while winding II on the inner stator teeth, the inner stator teeth, and the outer rotor constitute a Vernier machine.

1) For the magnetic-geared PM machine part, the salient poles of the inner rotor work as the flux modulator. Based on the basic principle of the flux-modulation theory [21], [22], the relationship of the pole-pair number of winding I, P_{WI}, PMs in the outer rotor, P_{or}, and the inner rotor, P_{ir}, is governed by:

$$P_{WI} = P_{or} - P_{ir} \tag{1}$$

It should be noted that the pole-pair number of the inner rotor is identical to the number of the inner rotor teeth. The relationship of the frequency of winding I, f_{WI}, the outer rotor speed, n_{or}, and the inner rotor speed, n_{or}, follows:

$$n_{WI}P_{WI} = n_{or}P_{or} - n_{ir}P_{ir} \tag{2}$$

$$f_{WI} = n_{WI}P_{WI}/60 = (n_{or}P_{or} - n_{ir}P_{ir})/60 \tag{3}$$

where n_{WI} is the equivalent rotating speed of the magnetic field that winding I links. As can be seen from eqs. (2) and (3), when the two rotors are rotating in a "contra-rotating" manner, the induced frequency in winding I will be increased, which is desirable for low-speed direct-drive wind power generation systems. Based on the law of energy conservation, the torque relationship can be written as follows:

$$n_{WI}T_{st\_WI} + n_{or}T_{or\_WI} + n_{ir}T_{ir\_WI} = 0 \tag{4}$$

where T_{st_WI}, T_{or_WI}, and T_{ir_WI} are the torques generated from winding I on the stator, the outer rotor, and the inner rotor, respectively. Based on the basic principle of magnetic gear [23], the torques transmitted from the stator to the outer rotor to the inner rotor are governed by:

$$\left.\begin{aligned} T_{or\_WI} &= -(P_{or}/P_{WI})\cdot T_{st\_WI} \\ T_{ir\_WI} &= -(P_{ir}/P_{or})\cdot T_{or\_WI} = (P_{ir}/P_{WI})\cdot T_{st\_WI} \end{aligned}\right\} \tag{5}$$

Hence, the gear ratios between the outer rotor and the stator, G_{or_WI}, the inner rotor and the outer rotor, G_{ir_or}, as well as the inner rotor and the stator, G_{ir_WI}, are as follows:

$$G_{or\_WI} = -P_{or}/P_{WI}; \quad G_{ir\_or} = -P_{ir}/P_{or}; \quad G_{ir\_WI} = P_{ir}/P_{WI} \tag{6}$$

TABLE I
MAIN PARAMETERS OF THE INVESTIGATED MACHINE

Parameter	Value
Number of slots for winding I	6
Number of slots for winding II	18
Number of pole-pairs of winding I	2
Number of pole-pairs of winding II	3
Number of PM pole-pairs in outer rotor	15
Number of steel segments in outer rotor	30
Number of salient poles in inner rotor	13

2) For the Vernier PM machine part, the inner stator teeth work as the flux modulator. It should be noted that this flux modulator is a static modulator and the inner stator slots are designed as open slots in order to improve the flux-modulation effect. The relationship of the pole-pair number of winding II, P_{WII}, the inner stator slot number, Q_{in}, and the pole-pair number of PMs in the outer rotor, P_{or}, is governed by:

$$P_{WII} = Q_{in} - P_{or} \tag{7}$$

The relationship of the frequency of winding II, f_{WII}, and the outer rotor speed, n_{or}, follows:

$$n_{WII}P_{WII} = n_{or}P_{or} \tag{8}$$

$$f_{WII} = n_{WII}P_{WII}/60 = n_{or}P_{or}/60 \tag{9}$$

It should be noted that for the Vernier machine part, there is no torque transmission to the inner rotor since the inner rotor is not involved in the energy transmission as demonstrated in eq. (7). Based on the law of energy conservation, the torque relationship can be written as follows:

$$n_{WII}T_{st\_WII} + n_{or}T_{or\_WII} = 0 \tag{10}$$

where T_{st_WII} and T_{or_WII} are the torques generated from winding II on the stator and the outer rotor, respectively. Substituting eq. (8) into eq. (10), the torque transmitted from the stator to the outer rotor is governed by:

$$T_{or\_WII} = -(P_{or}/P_{WII})\cdot T_{st\_WII} \tag{11}$$

Hence, the gear ratio between the outer rotor and the stator, G_{or_WII}, can be described as follows:

$$G_{or\_WII} = -P_{or}/P_{WII} \tag{12}$$

3) For the integrated flux-modulated machine including both the magnetic-geared PM machine part and the Vernier PM machine part, the torque relationship can be shown as follows:

$$\left.\begin{aligned} T_{st\_total} &= T_{st\_WI} + T_{st\_WII} && \text{(a)} \\ T_{or\_total} &= T_{or\_WI} + T_{or\_WII} \\ &= -(P_{or}/P_{WI})\cdot T_{st\_WI} + [-(P_{or}/P_{WII})\cdot T_{st\_WII}] && \text{(b)} \\ &= G_{or\_WI}T_{st\_WI} + G_{or\_WII}T_{st\_WII} \\ T_{ir\_total} &= T_{ir\_WI} \\ &= -(P_{ir}/P_{or})\cdot T_{or\_WI} = (P_{ir}/P_{WI})\cdot T_{st\_WI} && \text{(c)} \\ &= G_{ir\_or}T_{or\_WI} = G_{ir\_WI}T_{st\_WI} \end{aligned}\right\} \tag{13}$$

where T_{st_total}, T_{or_total}, and T_{ir_total} are the total torque generated from both winding I and winding II on the stator, the outer rotor, and the inner rotor, respectively. As can be seen from eq. (13.b), the total outer rotor torque, T_{or_total}, includes two

components, *i.e.*, the torque generated from the magnetic-geared machine part, T_{or_WI}, and the torque generated from the Vernier machine part, T_{or_WII}. It is interesting to note that compared to the two components (T_{st_WI} and T_{st_WII}) of the total torque on the stator [see eq. (13.a)], the two components (T_{or_WI} and T_{or_WII}) of the total torque on the outer rotor are increased by the corresponding gear ratios, *i.e.*, G_{or_WI} and G_{or_WII}. By contrast, the total inner rotor torque, T_{ir_total}, has only one single component, *i.e.*, the torque generated from the magnetic-geared machine part, T_{ir_WI}. This component is also increased by its gear ratio, *i.e.*, G_{ir_WI}, compared to the corresponding torque component on the stator, *i.e.*, T_{st_WI}.

In comparison with the conventional electric machines in which the electromagnetic torque generated on the rotor is always equal to that on the stator, the proposed flux-modulated machine works in a different manner, *viz.* both the magnetic-geared machine part and the vernier machine part work as a conventional electric machine with an "virtual reduction gear". This is the so-called "dual flux-modulation" phenomenon. More specifically, compared to the torque components generated on the stator, all torque components on the rotors are boosted by the "dual flux- modulation" effects. Hence, this machine is expected to exhibit high torque density, which is desirable for direct-drive wind power generation.

III. Decoupled Design of the Integrated Machine

Decoupling the two sets of windings is of paramount importance, since a part of the magnetic path of winding I is shared with that of winding II. Otherwise, additional voltages and circulating-current may be induced, which leads to control complexity and even deteriorates the whole system. Direct coupling between the two sets of stator windings means that the same stator magnetomotive force (MMF) harmonic component can be produced by both of the two winding sets. Through such MMF harmonic component, the two sets of windings can be coupled with each other. More specifically, when one set of windings is excited, an additional back-electromotive force (EMF) will be induced in the other winding set. Such coupling can be avoided by appropriately selecting the slot-pole combination, which will be illustrated in detail in this Section.

The flux linkage that links winding II due to the flux density produced by winding I, Ψ_{WII_WI}, can be expressed as follows:

$$\Psi_{WII\_WI} = l_{sk} R_g \int_0^{2\pi} N_{WII}(\theta) B_{WI}(\theta) d\theta \tag{14}$$

where l_{sk} is the stack length, R_g is the air-gap radius, θ is the angular position. $B_{WI}(\theta)$ is the resultant magnetic flux density distribution when winding I is excited without PM excitations, which can be expressed as follows:

$$B_{WI}(\theta) = \sum_{i=1,2,3\ldots} B_{WI\_i} \cos(iP_{WI}\theta - i\omega_{WI}t) \tag{15}$$

$N_{WII}(\theta)$ is the winding function of winding II, which can be expressed as follows:

$$N_{WII}(\theta) = \sum_{j=1,2,3\ldots} 2Q_{in}k_{wj}/(j\pi P_{WII}) \cdot \cos(jP_{WII}\theta) \tag{16}$$

where B_{WI_i} is the amplitude value of the i^{th} harmonic of the flux density distribution, ω_{WI} is the angular frequency of winding I, k_{wj} is the winding factor of the j^{th} harmonic.

As can be seen from eq. (14), the mutual flux linkage/ inductance between the two sets of windings can only consists of terms from the Fourier series representation of the winding function of winding II, $N_{WII}(\theta)$, and the magnetic flux density distribution due to winding I, $B_{WI}(\theta)$, which corresponds to the same absolute harmonic. More specifically, if S_{WI} and S_{WII} denote the set of absolute harmonics that have non-zero coefficients for the flux density distribution, $B_{WI}(\theta)$, and the winding function, $N_{WII}(\theta)$, then only harmonics in the intersection set, $S_{WI} \cap S_{WII}$, contribute to the mutual flux linkage/inductance. Hence, in order to decouple the two sets of windings, the aforementioned intersection set should be a null/empty set, *i.e.*, $S_{WI} \cap S_{WII} = \emptyset$.

It should be noted that the prerequisite for decoupling two sets of windings is unequal pole-pair numbers of two winding sets, i.e., $P_{WI} \neq P_{WII}$. Otherwise, the two sets of windings will always be coupled. Feasible slot-pole combinations to achieve decoupled windings are categorized as four scenarios: 1) both symmetrical windings, 2) asymmetrical winding I and symmetrical winding II, 3) symmetrical winding I and asymmetrical winding II, and 4) both asymmetrical windings.

A. Both Symmetrical Windings Scenario

The condition for symmetrical windings in three-phase machines, where the winding function and flux density distribution are featured with half-wave symmetry, mean no even-order harmonics as:

$$\left.\begin{aligned} Q_{out}/\mathrm{GCD}(Q_{out}, P_{WI}) &= 6i, \quad i = 1,2,3\ldots \\ Q_{in}/\mathrm{GCD}(Q_{in}, P_{WII}) &= 6j, \quad j = 1,2,3\ldots \end{aligned}\right\} \tag{17}$$

where Q_{out} is the outer stator slot number, and GCD is the greatest common divisor.

In this scenario, there is no even-order harmonic component in the flux density distribution, $B_{WI}(\theta)$, in eq. (15), and the winding function, $N_{WII}(\theta)$, in eq. (16). Hence, the sets of absolute harmonics, S_{WI} and S_{WII}, can be expressed as follows:

$$\left.\begin{aligned} S_{WI} &= \{s \,|\, s = P_{WI}(2i-1), \quad i = 1,2,3\ldots\} \\ S_{WII} &= \{s \,|\, s = P_{WII}(2j-1), \; j = 1,2,3\ldots\} \end{aligned}\right\} \tag{18}$$

where s is the element of the set S_{WI} or S_{WII}.

Decoupling the two sets of windings can be achieved if either of the following conditions is satisfied:

1) (P_{WI} is odd) & (P_{WII} is even).

If P_{WI} is odd and P_{WII} is even, then S_{WI} contains only odd numbers while S_{WII} contains only even numbers [see eq. (18)]. Hence, $S_{WI} \cap S_{WII} = \emptyset$, and the mutual flux linkage in eq. (14) will be zero.

2) (P_{WI} is even) & (P_{WII} is odd).

The rule for this condition can be proofed by the same way as the one above, *i.e.*, 1) (P_{WI} is odd) & (P_{WII} is even).

3) (P_{WI} and P_{WII} are both even) & ($P_{WII}/P_{WI}=a/b$, a and b are not both odd).

It should be noted that in this condition a/b is the irreducible fraction. $S_{WI}/P_{WI} = \{s|s = (2i\text{-}1), i=1,2,3...\}$, $S_{WII}/P_{WI} = \{s|s = P_{WII}(2j\text{-}1)/P_{WI}, j=1,2,3...\}$. As S_{WI}/P_{WI} contains only odd numbers, while S_{WII}/P_{WI} doesn't contain any odd number due to the fact that a and b are not both odd. Hence, $S_{WI}/P_{WI} \cap S_{WII}/P_{WI} = \emptyset$, and therefore $S_{WI} \cap S_{WII} = \emptyset$.

B. Asymmetrical Winding I and Symmetrical Winding II

If winding I is asymmetrical while winding II is symmetrical,

eq. (17) can be re-written as:

$$\left.\begin{aligned} Q_{out}/\mathrm{GCD}(Q_{out},P_{WI}) &\neq 6i, \quad i=1,2,3\ldots \\ Q_{in}/\mathrm{GCD}(Q_{in},P_{WII}) &= 6j, \quad j=1,2,3\ldots \end{aligned}\right\} \tag{19}$$

In this scenario, the sets of absolute harmonics, S_{WI} and S_{WII}, in eq. (18) can be re-expressed as follows:

$$\left.\begin{aligned} S_{WI} &= \{s \,|\, s = P_{WI} i, \quad i=1,2,3\ldots\} \\ S_{WII} &= \{s \,|\, s = P_{WII}(2j-1), \; j=1,2,3\ldots\} \end{aligned}\right\} \tag{20}$$

Decoupling the two sets of windings can be achieved if either of the following conditions is satisfied:

1) (P_{WI} is even) & (P_{WII} is odd).

If P_{WI} is even and P_{WII} is odd, then S_{WI} contains only even numbers, while S_{WII} contains only odd numbers [see eq. (20)]. Hence, $S_{WI} \cap S_{WII} = \emptyset$.

2) (P_{WI} and P_{WII} are both even) & ($P_{WI}/P_{WII}=a/b$, a is even and b is odd).

$S_{WI}/P_{WII} = \{s|s = P_{WI}(2i\text{-}1)/P_{WII}, i=1,2,3...\}$, $S_{WII}/P_{WII} = \{s|\ s = (2j\text{-}1), j=1,2,3...\}$. As S_{WI}/P_{WII} doesn't contain any odd number due to the fact that a is even and b is odd, while S_{WII}/P_{WII} contains only odd numbers. Hence, $S_{WI}/P_{WII} \cap S_{WII}/P_{WII} = \emptyset$, and therefore $S_{WI} \cap S_{WII} = \emptyset$.

C. Symmetrical Winding I and Asymmetrical Winding II

This scenario is similar to the previous one in Section III-B. Hence, similar conclusion can be drawn, i.e., decoupling the two sets of windings can be achieved if either of the following conditions is satisfied:

1) (P_{WI} is odd) & (P_{WII} is even).

2) (P_{WI} and P_{WII} are both even) & ($P_{WII}/P_{WI}=a/b$, a is even and b is odd).

D. Both Asymmetrical Windings Scenario

In this scenario, $S_{WI} \cap S_{WII} \neq \emptyset$, hence it is impossible to decouple the two sets of windings.

IV. Slot-Pole Combination Selection

Based on the theoretically analysed results above, optional slot-pole combinations are listed in Table II, where k_{w_WI} and k_{w_WII} are the winding factors of winding I and winding II, respectively. Numbers highlighted with shadow represent theoretically decoupled windings, while non-highlighted numbers represent coupled windings.

The induced voltages of two designs, i.e., a coupled design with 6-18-2-4 (Q_{out}-Q_{in}-P_{WI}-P_{WII}) and a decoupled design with 6-18-2-3, obtained by finite-element analysis (FEA) with only winding II is excited, are shown in Fig. 4. It should be noted that in order to avoid the effect from PMs, in these FEA models, PMs are removed. As can be seen, in the coupled design from Fig. 4(a), significant voltages of winding I are induced when only winding II is excited, which are called as "mutual-induced" voltages. By contrast, in the decoupled design from Fig. 4(b), the induced voltages of winding I are negligible when only winding II is excited. These results confirmed the fact that the two windings are decoupled in the decoupled design.

It should be noted that the slot-pole combinations with the number of pole-pairs of windings equal to unity are not included in Table II, since such machines exhibit the longest end-windings that will deteriorate the torque density. In addition, as can be seen from eq. (13), larger gear ratio of the output rotor to the associated winding is desirable to improve the output torque. Hence, the slot-pole combinations with the number of pole-pairs of windings larger than 5 (as indicated small gear ratio) are also not included in Table II. Accordingly, four slot-pole combinations with decoupled windings as well as G_{or_WI} and G_{or_WII} larger than 5, are selected and investigated. They are: 1) machine I with 6-18-2-3 (Q_{out}-Q_{in}-P_{WI}-P_{WII}), 2) machine II with 6-30-2-5, 3) machine III with 12-24-2-4, and 4) machine IV with 12-24-4-2. The main performance metrics of these four machines are compared and listed in Table III, where E_{WI_1} and E_{WII_1} are the fundamental component amplitude values of back-EMF of winding I and winding II, respectively, under the conditions of outer rotor rotating counter-clockwise at 200 r/min and inner rotor rotating clockwise at 300 r/min. THD is the associated total harmonic distortion, T_{avg_inner}, T_{rip_inner}, T_{avg_outer}, and T_{rip_outer} are the average torque and torque ripple of

TABLE II
Optional Slot-Pole Combinations for the Investigated Machine

Q_{out}	Q_{in}	P_{WI}	P_{WII}	P_{or}	P_{ir}	k_{w_WI}	k_{w_WII}	G_{or_WI}	G_{or_WII}
6	12	2	4	8	6	0.87	0.87	4	2
		2	5	7	5	0.87	0.93	3.5	1.4
	18	2	3	15	13	0.87	1	7.5	5
		2	4	14	12	0.87	0.95	7	3.5
		2	5	13	11	0.87	0.95	6.5	2.6
	24	2	4	20	18	0.87	1	10	5
		2	5	19	17	0.87	0.93	9.5	3.8
	30	2	4	26	24	0.87	0.95	13	6.5
		2	5	25	23	0.87	1	12.5	5
12	24	2	4	20	18	1	1	10	5
		2	5	19	17	1	0.93	9.5	3.8
		4	2	22	18	0.87	0.97	5.5	11
		4	5	19	15	0.87	0.93	4.75	3.8
		5	2	22	17	0.93	0.97	4.4	11
		5	4	20	15	0.93	1	4	5

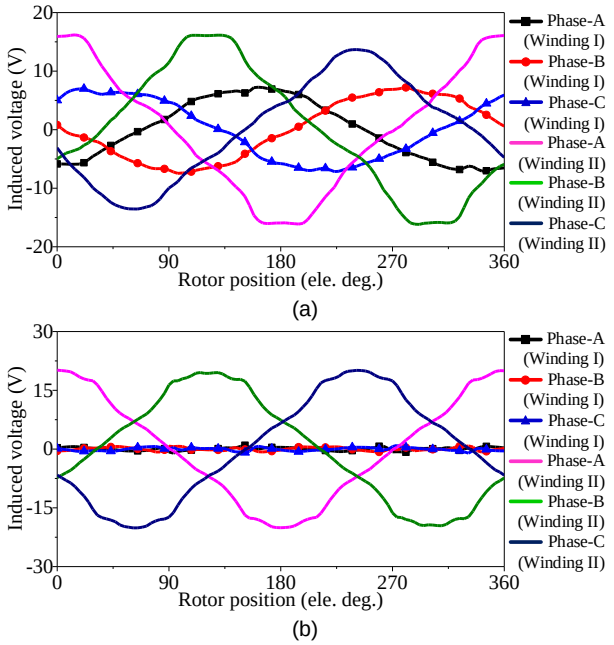

Fig. 4. Induced voltages when only winding II is excited. (a) Coupled design. (b) Decoupled design.

TABLE III
Main Performance Comparison of the Four Machines

	Machine I	Machine II	Machine III	Machine IV
$\boldsymbol{E_{WI\_1}}$ (V)	**26.94**	**30.39**	**34.45**	**12.13**
THD of E_{WI} (%)	3.17	2.57	2.91	1.96
$\boldsymbol{E_{WII\_1}}$ (V)	**32.58**	**26.36**	**28.46**	**39.59**
THD of E_{WII} (%)	4.25	2.61	4.32	3.12
$\boldsymbol{T_{avg\_outer}}$ (Nm)	**49.19**	**46.04**	**51.49**	**45.71**
T_{rip_outer} (%)	14.12	7.82	20.88	6.57
$\boldsymbol{T_{avg\_inner}}$ (Nm)	**-17.71**	**-20.84**	**-23.19**	**-7.52**
T_{rip_inner} (%)	13.31	4.93	8.05	65.33
P_{f_WI}	**0.52**	**0.27**	**0.49**	**0.43**
P_{f_WII}	**0.96**	**0.95**	**0.95**	**0.80**

the inner rotor and the outer rotor, respectively. P_{f_WI} and P_{f_WII} are the power factor of winding I and winding II, respectively. For a fair comparison, these four machines are with the same dimension, PM volume, and electric loading.

As can be seen, machine IV shows the lowest output torque on both the inner rotor and outer rotor. Machine II exhibits comparable output torque with machine I and machine III, but the power factor of winding I is the lowest. Even though machine III exhibits relative high output torque compared to machine I, the outer rotor torque ripple of machine III is highest. Since the outer rotor is the main output shaft connected to the main turbine [see Fig. 2], high torque ripple may lead to significant noise and vibration, or even malfunction of the whole system. Moreover, the power factors of both winding I and winding II of machine I are higher than those of machine III, which are preferable for wind power generation applications. On the other hand, the number of PMs in the outer rotor of machine I is smaller than that of machine III, *i.e.*, 30 (machine I) vs. 40 (machine III), which is desirable for achieving high mechanical strength of the outer rotor and high manufacturing feasibility in the given size, due to the fact that punched holes are required to hold the outer rotor as mentioned in [24], [25]. Accordingly, machine I is selected for further investigation and prototyping.

V. Comprehensive Performance Comparison

In order to comprehensively evaluate the electromagnetic performances of the integrated flux-modulated machine, quantitative performance comparison with an existing electric machine is conducted in this section. More details about the existing machine that serves as the benchmark machine in this paper, as shown in Fig. 5, can be found in [26], [27]. In the benchmark machine, winding I, steel segments, and the PMs in the inner rotor constitute a magnetic-geared machine, while winding II and the PMs in the outer rotor constitute a conventional PMSM. The torque density of this machine is improved by the enhanced flux-modulation effect due to the "flux-directional modulation" phenomenon. More specifically, the steel segments of the outer rotor work as the flux modulator to modulate the magnetic field excited by the PMs in the inner rotor, while the salient poles of the inner rotor can work as the flux modulator to modulate the magnetic field excited by the PMs in the outer rotor. For a fair comparison, the two machines share the same volume, slot fill factor, and electric loading. The specifications of the two machines are listed in Table IV.

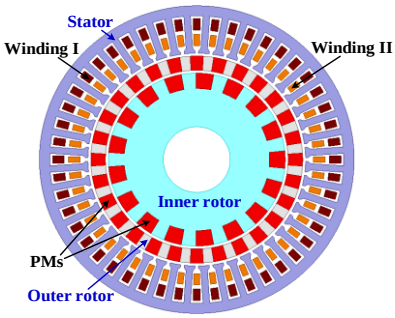

Fig. 5. Doubly-fed flux-bidirectional modulated machine [26].

TABLE IV
Specifications of the Two Electric Machines

Parameter	Benchmark Machine	Proposed Machine
Stator outer diameter (mm)	210	
Stator inner diameter (mm)	153.4	140
Outer air-gap length (mm)	1.0	
PM length in outer rotor (mm)	6.1	15
Inner air-gap length (mm)	1.0	
PM length in inner rotor (mm)	15.8	-
Inner rotor inner diameter (mm)	46	
Stack length (mm)	80	
Number of slots for winding I	48	6
Number of slots for winding II	48	18
Number of turns per phase of winding I	56	
Number of turns per phase of winding II	96	
Pole-pair number of winding I	11	2
Pole-pair number of winding II	28	3
Pole-pair number of PMs in outer rotor	28	15
Number of steel segments in outer rotor	28	30
Number of poles in inner rotor	17	13
Rated current of winding I (A)	18	
Rated current of winding II (A)	9	

A. Comparison of Air-Gap Flux Density

The magnetic flux density waveforms in the outer air-gap and the associated harmonic spectrum of the two investigated machines are shown in Fig. 6. As can be seen, for the magnetic-geared machine part of the two machines, the working harmonic amplitude value of the benchmark machine (11^{th} harmonic) is higher than that of the proposed machine (2^{nd} harmonic), *i.e.*, $B_g(11^{th}) = 0.25$ T vs. $B_g(2^{nd}) = 0.14$ T. However, the equivalent flux density to produce torque, *i.e.*, $G_{or\_WI} \times B_g$, of the benchmark machine is: (28/11)×0.25 T=0.64 T, which is lower than that of the proposed machine, *i.e.*, (15/2)×0.14 T=1.05 T. For the PMSM part of the benchmark machine, there is only one working harmonic, *i.e.*, the 28^{th} harmonic = 0.72 T. By contrast, for the Vernier part of the proposed machine, there are three main working harmonics, *i.e.*, the 3^{rd} harmonic $B_g(3^{rd})$ = 0.21 T, the 15^{th} harmonic $B_g(15^{th})$ = 0.79 T, and the 33^{rd} harmonic $B_g(33^{rd})$ = 0.31 T. The equivalent flux density of the proposed machine is: $G_{or\_WII} \times B_g(3^{rd}) + B_g(15^{th}) - P_{or}/(P_{or} + Q_{in}) \times B_g(33^{rd})$ = (15/3) × 0.21 + 0.79 - (15/33) × 0.31 = 1.70 T, which is much larger than that of the PMSM part of the benchmark machine. Hence, the proposed machine is expected to exhibit higher back-EMF and output torque than those of the benchmark machine.

B. Comparison of Back-EMF

The no-load back-EMF waveforms of the two machines under the rated condition of the outer rotor rotating counter-

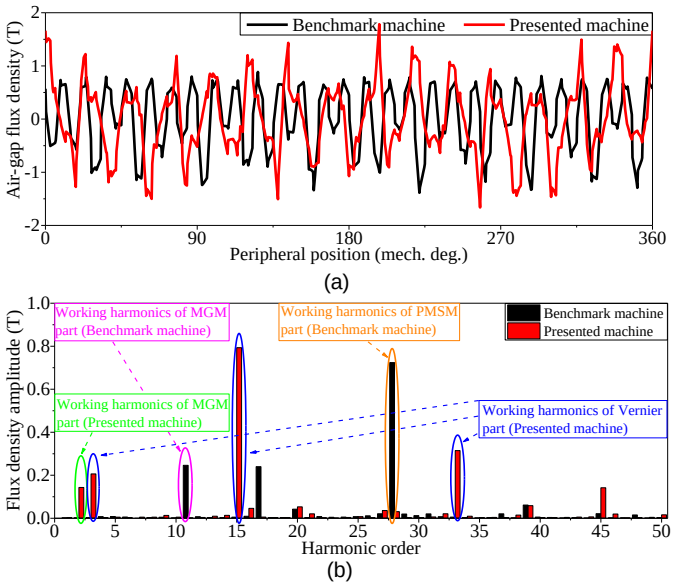

Fig. 6. Flux densities in outer air-gap. (a) Waveforms. (b) Harmonic spectrum (MGM stands for magnetic-geared machine).

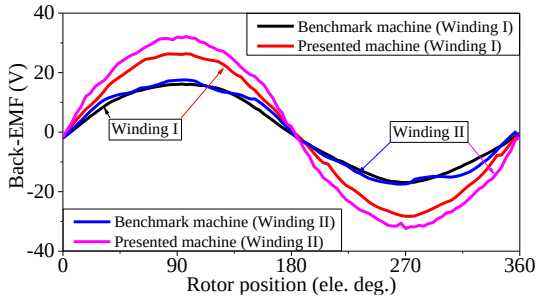

Fig. 7. Back-EMF waveforms.

clockwise at 200 r/min and the inner rotor rotating clockwise at 300 r/min, are shown in Fig. 7. The detailed results including the fundamental component amplitude value for winding I and winding II, E_{WI_1} and E_{WII_1}, as well as the total harmonic distortion, *THD*, are listed in Table V. As can be seen, compared to the benchmark machine, with the same number of turns per phase, the back-EMF fundamental component of winding I of the proposed machine is significantly improved from 13.62 V to 26.94 V, while the *THD* is reduced from 5.08% to 3.17%. The back-EMF fundamental component of winding II of the proposed machine is also improved from 17.46 V to 32.58 V, while the *THD* is reduced from 7.81% to 4.25%.

C. Comparison of Torque Characteristics

The torque profiles of the two machines under the rated operating conditions of 18 A and 9 A currents excited in winding I and winding II, respectively, are shown in Fig. 8. As can be seen, the average torque on the outer rotor, T_{avg_outer}, of the proposed machine is significantly improved compared to the benchmark machine, *i.e.*, 49.19 Nm vs. 30.95 Nm, while the associated torque ripple, T_{rip_outer}, of the proposed machine is lower than that of the benchmark machine, *i.e.*, 14.12% vs. 19.87%. In addition, the average torque on the inner rotor, T_{avg_inner}, of the proposed machine is also much higher than that of the benchmark machine, *i.e.*, 17.71 Nm vs. 10.88 Nm, while the associated torque ripple, T_{rip_inner}, comparison is 13.31%

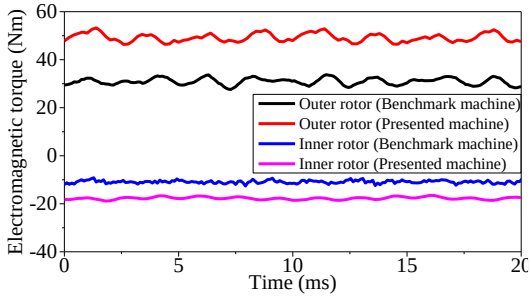

Fig. 8. Electromagnetic torques.

TABLE V
PERFORMANCE COMPARISONS OF THE TWO ELECTRIC MACHINES

Performance	Benchmark Machine	Proposed Machine
E_{WI_1} (V)	**13.62**	**26.94**
THD of E_{WI} (%)	5.08	3.17
E_{WII_1} (V)	**17.46**	**32.58**
THD of E_{WII} (%)	7.81	4.25
T_{avg_outer} (only winding I excited) (Nm)	**15.83**	**20.56**
T_{rip_outer} (only winding I excited) (%)	47.25	32.45
T_{avg_inner} (only winding I excited) (Nm)	**-9.98**	**-17.87**
T_{rip_inner} (only winding I excited) (%)	35.81	11.79
T_{avg_outer} (only winding II excited) (Nm)	**15.43**	**29.55**
T_{rip_outer} (only winding II excited) (%)	36.11	22.54
T_{avg_inner} (only winding II excited) (Nm)	**-0.60**	**0.31**
T_{rip_inner} (only winding II excited) (%)	-	-
T_{avg_outer} (both windings excited) (Nm)	**30.95**	**49.19**
T_{rip_outer} (both windings excited) (%)	19.87	14.12
T_{avg_inner} (both windings excited) (Nm)	**-10.88**	**-17.71**
T_{rip_inner} (both windings excited) (%)	31.50	13.31
Power factor in winding I	0.84	0.52
Power factor in winding II	0.88	0.96
Copper losses (W)	156.01	156.01
Core losses (W)	39.02	56.22
PM eddy-current losses (W)	13.04	4.00
Efficiency (%)	82.63	88.01
Output power (W)	989.95	1586.49
Power density (kW/L)	0.36	0.59
PM consumption (L)	0.39	0.19

(proposed machine) vs. 31.50% (benchmark machine).

More detailed results are listed in Table V. As can be seen, in the case when only winding I excited, i.e., the magnetic-geared machine part for both the benchmark machine and the proposed machine, both the outer rotor and inner rotor average torque values of the proposed machine are higher than those of the benchmark machine, *i.e.*, 20.56 Nm vs. 15.83 Nm for the outer rotor, and 17.87 Nm vs. 9.98 Nm for the inner rotor, respectively. The ratio values of the outer rotor average torque to the inner rotor average torque of the proposed machine and the benchmark machine are 20.56/17.87≈1.15 and 15.83/9.98 ≈1.59, which are consistent with their gear ratios between the outer rotor to the inner rotor, *i.e.*, 15/13≈1.15 and 28/17=1.65, respectively. The associated torque ripple results of the proposed machine are lower than those of the benchmark machine, *i.e.*, 32.45% vs. 47.25% for the outer rotor, and 11.79% vs. 35.81% for the inner rotor, respectively. In the case when only winding II excited, the outer rotor average torque of the proposed machine is also higher than that of the benchmark machine, *i.e.*, 29.55 Nm vs. 15.43 Nm, while the torque ripple of the proposed machine is lower than that of the benchmark machine, *i.e.*, 22.54% vs. 36.11%. The inner rotor average torque results of both the two machines are almost zero, since the inner rotor is not coupled with winding II for both of the two

machines.

D. Other Performance Comparison and Discussion.

Besides the flux density, back-EMF, and torque characteristics mentioned in previous subsections, other performance metrics of the two machines including power factor, losses, efficiency, *etc*., are compared in Table V.

As can be observed, the power factor of winding I of the proposed machine is lower than that of the benchmark machine, *i.e.*, 0.52 vs. 0.84, while the power factor of winding II of the proposed machine is higher than that of the benchmark machine, *i.e.*, 0.96 vs. 0.88. The relatively low power factor of winding I of the proposed machine is due to the high gear ratio between the output rotor and the associated winding in the magnetic-geared machine part. More specifically, the gear ratio between the outer rotor (output rotor) and winding I of the proposed machine is G_{or_WI} = 15/2=7.5, while the gear ratio between the inner rotor (output rotor) to winding I of the benchmark machine is G_{ir_WI} = 17/11≈1.55.

On the other hand, the efficiency of the proposed machine is higher than that of the benchmark machine, *i.e.*, 88.01% vs. 82.63%. Furthermore, compared to the benchmark machine, the power density of the proposed machine is improved from 0.36 kW/L to 0.59 kW/L. Moreover, the PM consumption of the proposed machine is significantly reduced from 0.39 L to 0.19 L, which indicates that the proposed machine exhibits better PM utilization ratio.

In summary, the proposed machine outperforms the benchmark machine in terms of higher back-EMF in both winding I and winding II, higher electromagnetic torque on both the outer rotor and inner rotor, higher efficiency, improved torque/power density and PM utilization ratio. The major limitation of the proposed machine is the relatively low power factor of winding I, due to the high gear ratio in the magnetic-geared machine part. This issue can be overcome by the reactive power compensation techniques [28].

VI. Prototype and Experimental Validation

In order to verify the theoretical analysis and simulation results in this paper, the prototype of the integrated flux-modulated machine is fabricated and tested, as shown in Fig. 9.

The no-load back-EMF waveforms under the rated conditions of the outer rotor rotating counter-clockwise at 200 r/min and the inner rotor rotating clockwise at 300 r/min, are shown in Fig. 10. As can be seen, the experimental results are in good agreement with the FEA simulated results. More specifically, the discrepancy of the fundamental component amplitude values of the simulated and measured phase-A back-EMFs of the outer winding [see Fig. 10(a)] is 1.6%, *i.e.*, 26.95 V (simulated) vs. 26.51 V (measured), while the *THD* results of the phase-A back-EMF waveforms are 3.17% (simulated) vs. 5.86% (measured). The discrepancy of the fundamental component amplitude value of the simulated and measured phase-A back-EMFs of the inner winding [see Fig. 10(b)] is 2.1%, *i.e.*, 32.58 V (simulated) vs. 31.91 V (measured), while the *THD* results of the phase-A back-EMF waveforms are 4.25% (simulated) vs. 6.23% (measured).

The comparison of the FEA predicted and measured inner and outer rotor average torques versus currents, is shown in Fig. 11.

As can be seen, the measured torque results are also in acceptable agreement with those predicted by FEA. More specifically, the discrepancy of the simulated and measured outer rotor torque under the rated conditions is 16.14%, *i.e.*,

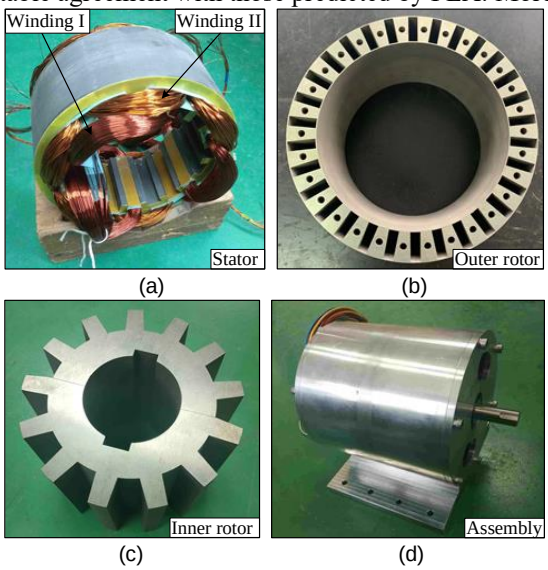

Fig. 9. Prototype. (a) Stator. (b) Outer rotor. (c) Inner rotor. (d) Assembly.

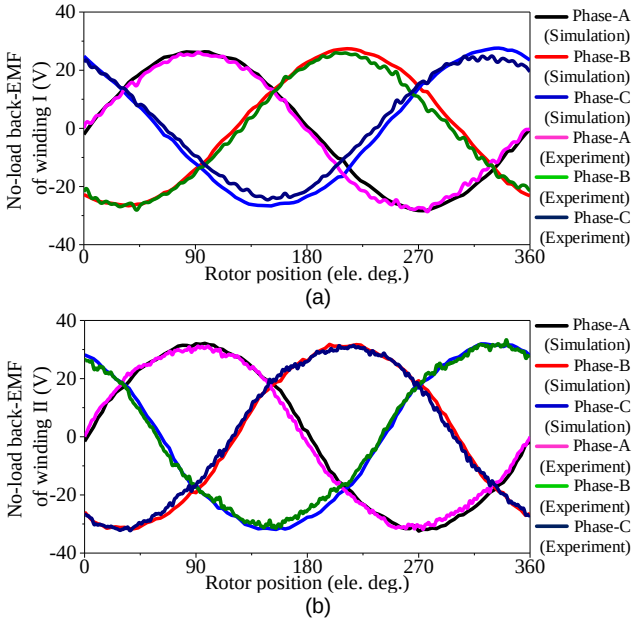

Fig. 10. Experimental results of no-load back-EMF in comparison with simulation results. (a) Winding I. (b) Winding II.

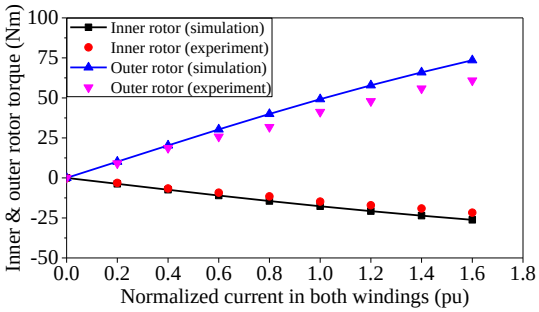

Fig. 11. Experimental results of rotor average toques versus currents.

49.19 Nm (simulated) vs. 41.25 Nm (measured), while the discrepancy of the inner rotor torque under the rated condition is 16.43%, *i.e.*, -17.71 Nm (simulated) vs. -14.80 Nm (measured).

VII. Conclusion

An integrated flux-modulated machine featured with dual flux-modulation phenomenon for wind power generation is proposed and investigated in this paper. The integrated flux-modulated machine consists of two parts, *i.e.*, magnetic-geared PM machine part and Vernier PM machine part. The magnetic-geared machine part is formed by winding I, PMs in the outer rotor and the inner rotor, where the salient inner rotor teeth work as the flux modulator. The Vernier machine part is formed by winding II, the inner stator teeth and the outer rotor, where the inner stator teeth work as the flux modulator. Hence, the so-called "dual flux-modulation" phenomenon exists in this machine. Due to the "dual flux-modulation" effect, the integrated flux-modulated machine exhibits the advantage of high torque/power density, which is suitable for direct-drive contra-rotating wind power generation systems. The operating principle of the integrated flux-modulated machine is demonstrated in detail. Decoupled design of the two sets of windings is investigated, and a general rule to achieve decoupled windings by appropriate slot-pole combination selection is illustrated. The advantages of the proposed machine are confirmed in comparison with a benchmark machine. Finally, the integrated flux-modulated machine is prototyped, and the experimental results verify the feasibility and validity of the operating principle and the FEA predictions of the proposed machine.

References

[1] F. Blaabjerg, R. Teodorescu, M. Liserre, and A. V. Timbus, "Overview of control and grid synchronization for distributed power generation systems," *IEEE Trans. Ind. Electron.*, vol. 53, no. 5, pp. 1398–1409, Oct. 2006.

[2] V. Yaramasu, B. Wu, P. C. Sen, S. Kouro, and M. Narimani, "High-power wind energy conversion systems: state-of-the-art and emerging technologies," *Proc. IEEE*, vol. 103, no. 5, pp. 740–788, May 2015.

[3] A. D. Gerlando, G. Foglia, M. F. Iacchetti, and R. Perini, "Axial flux PM machines with concentrated armature windings: design analysis and test validation of wind energy generators," *IEEE Trans. Ind. Electron.*, vol. 58, no. 9, pp. 3795–3805, Sep. 2011.

[4] P. Han, M. Cheng, Y. Jiang, and Z. Chen, "Torque/power density optimization of a dual-stator brushless doubly-fed induction generator for wind power application," *IEEE Trans. Ind. Electron.*, vol. 64, no. 12, pp. 9864–9875, Dec. 2017.

[5] I. Erlich, F. Shewarega, C. Feltes, F. W. Koch, and J. Fortmann, "Offshore wind power generation technologies," *Proc. IEEE*, vol. 101, no. 4, pp. 891–905, Apr. 2013.

[6] Z. Chen, J. M. Guerrero, and F. Blaabjerg, "A review of the state of the art of power electronics for wind turbines," *IEEE Trans. Power Electron.*, vol. 24, no. 8, pp. 1859–1875, Aug. 2009.

[7] J. Ojeda, M. G. Simoes, G. Li, and M. Gabsi, "Design of a flux-switching electrical generator for wind turbine systems," *IEEE Trans. Ind. Appl.*, vol. 48, no. 6, pp. 1808–1816, Nov. 2012.

[8] H. Chen, A. M. EL-Refaie, and N. A. O. Demerdash, "Flux-switching permanent magnet machines: a review of opportunities and challenges-part II: design aspects, control, and emerging trends," *IEEE Trans. Energy Convers.*, vol. 35, no. 2, pp. 699–713, Jun. 2020.

[9] D. Li, Y. Gao, R. Qu, J. Li, Y. Huo, and H. Ding, "Design and analysis of a flux reversal machine with evenly distributed permanent magnets," *IEEE Trans. Ind. Appl.*, vol. 54, no. 1, pp. 172–183, Jan. 2018.

[10] B. Kim, "Design method of a direct-drive permanent magnet vernier generator for a wind turbine system," *IEEE Trans. Ind. Appl.*, vol. 55, no. 5, pp. 4665–4675, Sep. 2019.

[11] L. Jian, K. T. Chau, and J. Z. Jiang, "A magnetic-geared outer-rotor permanent-magnet brushless machine for wind power generation," *IEEE Trans. Ind. Appl.*, vol. 45, no. 3, pp. 954–962, 2009.

[12] A. B. Kjaer, S. Korsgaard, S. S. Nielsen, L. Demsa, and P. O. Rasmussen, "Design, fabrication, test, and benchmark of a magnetically geared permanent magnet generator for wind power generation," *IEEE Trans. Energy Convers.*, vol. 35, no. 1, pp. 24–32, Mar. 2020.

[13] P. M. Tlali, S. Gerber, and R.-J. Wang, "Optimal design of an outer-stator magnetically geared permanent magnet machine," *IEEE Trans. Magn.*, vol. 52, no. 2, pp. 1–10, Feb. 2016.

[14] H. Chen, Y. Zuo, K. T. Chau, W. Zhao, and C. H. T. Lee, "Modern electric machines and drives for wind power generation: a review of opportunities and challenges," *IET Renew. Power Gener.*, vol. n/a, no. n/a, pp. 1–24, Feb. 2021.

[15] J. M. Crider and S. D. Sudhoff, "An inner rotor flux-modulated permanent magnet synchronous machine for low-speed high-torque applications," *IEEE Trans. Energy Convers.*, vol. 30, no. 3, pp. 1247–1254, Sep. 2015.

[16] C. Liu, K. T. Chau, and Z. Zhang, "Novel design of double-stator single-rotor magnetic-geared machines," *IEEE Trans. Magn.*, vol. 48, no. 11, pp. 4180–4183, Nov. 2012.

[17] X. Zhao and S. Niu, "Design and optimization of a new magnetic-geared pole-changing hybrid excitation machine," *IEEE Trans. Ind. Electron.*, vol. 64, no. 12, pp. 9943–9952, Dec. 2017.

[18] C. Shin, "Multi-Unit rotor blade system integrated wind turbine." U.S. Patent No. 5,876,181. Mar. 1999.

[19] S. N. Jung, T.-S. No, and K.-W. Ryu, "Aerodynamic performance prediction of a 30kW counter-rotating wind turbine system," *Renew. Energy*, vol. 30, no. 5, pp. 631–644, Apr. 2005.

[20] P. S. Kumar, A. Abraham, R. J. Bensingh, and S. Ilangovan, "Computational and experimental analysis of a counter-rotating wind turbine system," *J. Sci. Ind. Res.*, vol. 72, no. 5, pp. 300–306, May 2013.

[21] K. Atallah, S. D. Calverley, and D. Howe, "Design, analysis and realisation of a high-performance magnetic gear," *IEE Proc. - Electr. Power Appl.*, vol. 151, no. 2, pp. 135–143, Mar. 2004.

[22] J. Bai, P. Zheng, C. Tong, Z. Song, and Q. Zhao, "Characteristic analysis and verification of the magnetic-field-modulated brushless double-rotor machine," *IEEE Trans. Ind. Electron.*, vol. 62, no. 7, pp. 4023–4033, Jul. 2015.

[23] G. Jungmayr, J. Loeffler, B. Winter, F. Jeske, and W. Amrhein, "Magnetic gear: radial force, cogging torque, skewing, and optimization," *IEEE Trans. Ind. Appl.*, vol. 52, no. 5, pp. 3822–3830, Sep. 2016.

[24] D. Li, R. Qu, and T. A. Lipo, "High-power-factor vernier permanent-magnet machines," *IEEE Trans. Ind. Appl.*, vol. 50, no. 6, pp. 3664–3674, Nov. 2014.

[25] X. Ren, D. Li, R. Qu, W. Kong, X. Han, and T. Pei, "Analysis of spoke-type brushless dual-electrical-port dual-mechanical-port machine with decoupled windings," *IEEE Trans. Ind. Electron.*, vol. 66, no. 8, pp. 6128–6140, Aug. 2019.

[26] Y. Wang, S. Niu, and W. Fu, "Electrical-continuously variable transmission system based on doubly fed flux-bidirectional modulation," *IEEE Trans. Ind. Electron.*, vol. 64, no. 4, pp. 2722–2731, Apr. 2017.

[27] X. Luo and S. Niu, "A novel contra-rotating power split transmission system for wind power generation and its dual MPPT control strategy," *IEEE Trans. Power Electron.*, vol. 32, no. 9, pp. 6924–6935, Sep. 2017.

[28] X. She, A. Q. Huang, F. Wang, and R. Burgos, "Wind energy system with integrated functions of active power transfer, reactive power compensation, and voltage conversion," *IEEE Trans. Ind. Electron.*, vol. 60, no. 10, pp. 4512–4524, Oct. 2013.